

By acceptance of this article, the publisher or recipient acknowledges the U.S. Government's right to retain a nonexclusive, royalty-free license in and to any copyright covering the article.

CONF - 800205 - - 7

**MASTER**

## CRYSTAL DEFECT STUDIES USING X-RAY DIFFUSE SCATTERING

B. C. Larson

Solid State Division, Oak Ridge National Laboratory  
Oak Ridge, Tennessee 37830

### DISCLAIMER

This book was prepared in an account of work sponsored by an agency of the United States Government. Neither the United States Government nor any agency thereof, nor any of their employees, makes a warranty, express or implied, or assumes any legal liability or responsibility for the accuracy, completeness, or usefulness of any information, apparatus, product, or process disclosed, or represents that its use would not infringe privately owned rights. Reference herein to any specific commercial product, process, or service by trade name, trademark, manufacturer, or otherwise, does not necessarily constitute or imply its endorsement, recommendation, or favoring by the United States Government or any agency thereof. The views and opinions of authors expressed herein do not necessarily state or reflect those of the United States Government or any agency thereof.

### Summary

Microscopic lattice defects such as point (single atom) defects, dislocation loops, and solute precipitates are characterized by local electronic density changes at the defect sites and by distortions of the lattice structure surrounding the defects. The effect of these interruptions of the crystal lattice on the scattering of x-rays is considered in this paper, and examples are presented of the use of the diffuse scattering to study the defects.

X-ray studies of self-interstitials in electron irradiated aluminum and copper are discussed in terms of the identification of the interstitial configuration. Methods for detecting the onset of point defect aggregation into dislocation loops are considered and new techniques for the determination of separate size distributions for vacancy loops and interstitial loops are presented. Direct comparisons of dislocation loop measurements by x-rays with existing electron microscopy studies of dislocation loops indicate agreement for larger size loops, but x-ray measurements report higher concentrations in the smaller loop range. Methods for distinguishing between loops and three-dimensional precipitates are discussed and possibilities for detailed studies of precipitates are considered. A comparison of dislocation loop size distributions obtained from integral diffuse scattering measurements with those from TEM show a discrepancy in the smaller sizes similar to that described above.

\* Research sponsored by Union Carbide Corporation under contract W-7405-eng-26 with the U.S. Department of Energy.

B. C. Larson

## Introduction

Detailed use of x-ray diffuse scattering around Bragg reflections for the study of small lattice defects has increased considerably in the last ten years. Analytical work by Krivoglas (1), Dederichs (2) and Trinkaus (3) was instrumental in developing the present form of the theory for defect clusters, and radiation damage investigations (4-8) have been responsible for much of the experimental activity in this field. Alternate formulations of defect diffuse scattering exist (9) and provide powerful tools for the study of lattice structure and defects; however, in the limited scope of this paper, only the former treatment will be discussed because of its adaptability to the case of sizeable clusters. No attempt is made to give a comprehensive review of the work in this field. Rather, it is the aim of this paper to indicate the range of information that can be obtained from this scattering and the methods used in this process. A brief review of the mathematical framework will be given, a short discussion of the experimental requirements for diffuse scattering measurements will be presented, and examples of point defect, dislocation loop and solute precipitate studies will be given. The primary purpose of the results shown will be to illustrate the techniques rather than to discuss the physical interpretations. Where meaningful, comparisons with electron microscopy results will be made in order to establish a reference point. Finally, more general comments and conclusions relative to the applicability and limitations of the x-ray method will be discussed.

## Theoretical Framework

The theory of diffuse scattering from lattice defects has been discussed in some detail in a number of papers (1-3), and only an outline of the theoretical results required to interpret the scattering results will be given here. The scattering cross-section for randomly distributed defects in a crystal lattice is given by

$$\frac{d\sigma}{d\Omega}(\vec{k}) = (r_e f)^2 |A(\vec{k})|^2 \quad (1)$$

where the scattering vector  $\vec{k} = \vec{h} + \vec{q}$  specifies the measuring position in terms of a reciprocal lattice vector  $\vec{h}$  and a position  $\vec{q}$  relative to  $\vec{h}$ .  $r_e$  is the classical electron radius,  $f_h$  is the atomic scattering factor of the host lattice (including thermal and polarization effects), and  $A(\vec{k})$  is the scattering amplitude. The scattering amplitude contains all the physics pertaining to the defect structure and, in general, is composed of the scattering from the defect atoms (sometimes called Laue or direct scattering) and the scattering generated as a result of the displacement of the atoms surrounding the defect site. The form of this is

$$A(\vec{k}) = \sum_j e^{i\vec{k} \cdot \vec{r}_j^d} + \sum_j e^{i\vec{q} \cdot \vec{r}_j} (e^{i\vec{k} \cdot \vec{S}_j} - 1) \quad (2)$$

where  $\vec{r}_j^d$  is the position of the defect atom(s) and  $\vec{S}_j$  is the displacement of the  $j^{\text{th}}$  lattice atom from its undistorted position  $\vec{r}_j$ . The -1 in the second term is inserted to remove the scattering from the periodic lattice (Bragg reflections, tails of Bragg reflections) so that for  $\vec{S}_j = 0$ , the distortion term vanishes.

For single interstitials,  $A(\vec{k})$  is given by (4)

$$A(\vec{k})_I = e^{i\vec{k}\cdot\vec{r}_I} + \sum_j e^{i\vec{q}\cdot\vec{r}_j} (e^{i\vec{k}\cdot\vec{s}_j} - 1) \quad (3)$$

where  $\vec{r}_I$  is the position of the interstitial atom. The first term represents the Laue scattering and the second represents the scattering from the distortion field around the defect. The entirely analogous amplitude for dislocation loops is given by

$$A(\vec{k})_L = \sum_j e^{i\vec{k}\cdot\vec{r}_j^L} + \sum_j e^{i\vec{q}\cdot\vec{r}_j} (e^{i\vec{k}\cdot\vec{s}_j} - 1) \quad (4)$$

in which  $\vec{r}_j^L$  are the positions of the atoms in the dislocation loop. The sign of  $\vec{s}_j$  reverses on going from interstitial to vacancy loops and  $\vec{r}_j^L$  changes to account for an intrinsic rather than extrinsic loop. An additional factor of  $(-1)$  must be included in the vacancy loop Laue scattering to represent the absence of atoms rather than the presence of additional atoms. The scattering amplitude for coherent precipitates of atoms with scattering factor  $f_p$  in a host lattice of scattering factor  $f_h$  is given by

$$A(K)_p = \sum_j e^{i\vec{q}\cdot\vec{r}_j^p} \frac{f_p}{f_h} (e^{i\vec{k}\cdot\vec{s}_j} - 1) + \sum_j e^{i\vec{q}\cdot\vec{r}_j} (e^{i\vec{k}\cdot\vec{s}_j} - 1). \quad (5)$$

The first sum runs over the  $\vec{r}_j^p$  positions of the precipitate atoms and the second sum over the host atoms outside the precipitate volume. Since there are no additional (or missing) lattice sites involved, the Laue term as in Eqs. (3,4) does not appear as such; however, the first term in Eq. (5) can be considered the Laue scattering here. The factor  $f_p/f_h$  occurs because we are replacing host atoms of scattering  $f_h$  with ones of scattering  $f_p$ . For simplicity here, the change in the host scattering due to the loss of the randomly distributed precipitating atoms through precipitation has been neglected.

Eqs. (3,4,5) require detailed knowledge of the displacements around the defect sites and require numerical integrations of the lattice sums for evaluation. For detailed studies, this is true in general; however, analytic approximations are available that provide symmetry information and the overall form of the scattering in particular regions (3). When  $K \cdot S \ll 1$ , the distortion scattering can be expanded so that

$$A^H(\vec{k}) \approx e^{i\vec{q}\cdot\vec{r}} (i\vec{k}\cdot\vec{s}) = i\vec{k}\cdot\vec{s}(\vec{q}) \quad (6)$$

which is the so called Huang diffuse scattering amplitude. Even in cases where  $\vec{k}\cdot\vec{s}(\vec{r}) \geq 1$  out to a radius of  $r=R_c$  around a clustered defect, Eq. (6) can remain a useful result for  $q < 1/R_c$  (i.e. close to the reciprocal lattice point). For the small  $q$  region  $A^H(\vec{k})$  can be calculated analytically for arbitrary lattice anisotropy as (6)

$$|A^H(\vec{k})|^2 = \frac{h^2}{q^2} (\gamma_1\pi_1 + \gamma_2\pi_2 + \gamma_3\pi_3) \quad (7)$$

where the  $\gamma$ 's are functions of the elastic constants,  $\vec{h}$ , and  $\vec{q}$ . The  $\pi$ 's contain the defect characteristics in the form of the dipole-force tensor.  $\pi_1$  is proportional to  $(\Delta V)^2$  where  $\Delta V$  is the volume change due to the defect and  $\pi_2$  and  $\pi_3$  are related to the anisotropy (relative to spherical or cubic symmetry) of the distortion field around the defect site.

The next approximation to Eq. (2), obtained by including all the even orders of  $\vec{K} \cdot \vec{S}$  leads to

$$|A(\vec{K})|^2 \approx |A^H(\vec{K})|^2 - 2i A^H(\vec{K}) L(\vec{K}) \quad (8)$$

where  $L(\vec{K})$  is essentially the Debye-Waller factor associated with the defect. Since  $A^H(\vec{K})$  is antisymmetric in  $q$  and  $L(\vec{K})$  is symmetric in  $q$ , Eq. (8) indicates the important result that the scattering for  $q < 1/R_c$  contains a term proportional to  $(\Delta V)^2 h^2/q^2$  and a term proportional to  $(\Delta V)h/q$  so that the symmetric average  $((I(q) + I(-q))/2)$  of the intensity parallel and anti-parallel to  $\vec{h}$  determines  $(\Delta V)^2$  and the sign of the asymmetry determines if the defect contracts (vacancy like) or expands (interstitial like) the lattice. Higher scattering intensities for  $q > 0$  imply interstitial like defects where the displacements are outward. A rough approximation for  $L(\vec{K})$  can be given for  $q < 1/R_c$  as (6)

$$L(\vec{K}) \approx \frac{|h\Delta V|^{3/2}}{10V_c} \quad (9)$$

where  $V_c$  is one atomic volume.

The region of  $q > 1/R_c$ , for which the above approximations break down, no longer retains the  $1/q^2$  falloff but decreases more like  $1/q^4$ , as a result of the increased interferences. An analytic approximation for  $q > 1/R_c$  is given by (6,10)

$$|A^A(\vec{K})|^2 \approx \frac{h|\Delta V|}{4\pi V_c q} \phi(\vec{q}/q). \quad (10)$$

$\phi(\vec{q}/q)$  is, in general, a function of angle but has an average about 150, which is applicable for both spherical defects and dislocation loops. This amplitude has been given the superscript A (Asymptotic diffuse scattering) and comes mainly from the highly distorted region near the defect site where  $\vec{K} \cdot \vec{S} \geq 1$ .

Eqs. (8,10) provide the basis for understanding the general features of defect diffuse scattering near Bragg reflections. However, for detailed quantitative information, direct numerical integration of Eqs. (3,4,5) is necessary. These calculations will not be discussed in detail in this paper, although the results of such calculations play an essential role in the results to be discussed later (11,12).

The above discussion applies to the usual differential diffuse scattering measurements in which the measured intensity in symmetric geometry is related to the scattering cross-section of Eq. (1) by

$$I(\vec{K}) = \frac{I_0}{2\mu_0} \sum_i C_i \frac{d\sigma_i(\vec{K})}{d\Omega} \Delta\Omega \quad (11)$$

where  $I_0$  is the incident beam power,  $\mu_0$  is the linear absorption coefficient,  $C_i$  is the volume concentration of the  $i^{\text{th}}$  defect and  $\Delta\Omega$  is the solid angle subtended at the detector. These measurements correspond to the geometry sketched in Fig. (1a). A useful variation of the scattering geometry is shown in Fig. (1b) in which the scattering from dislocation loops is studied using a wide-open (that is, no collimator defining the diffracted beam)

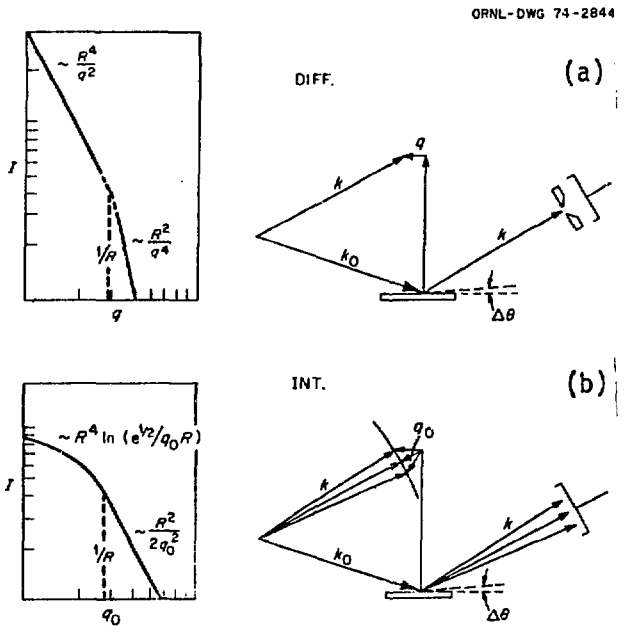


Fig. 1- Schematic view of Differential and Integral diffuse scattering geometries and results.

detector (13). Under the approximation of isotropic scattering (which is reasonable for loops in cubic materials), the intensity averaged at  $\pm q_0$  ( $I^S(q_0)$ ) for the Integral diffuse scattering is given by (6)

$$I^S(q_0) = \frac{I_0 (r_e f)^2}{2L_0} \left(\frac{h}{k}\right)^2 2\pi \sum_i C_i \left(\frac{b\pi R_i^2}{V_c}\right)^2 \left\{ \begin{array}{l} \ln(e^{1/2} \alpha / q_0 R_i) \\ \frac{\alpha^2}{2q_0^2 R_i^2} \end{array} \right\} \quad (12)$$

where  $k = 2\pi/\text{wavelength}$ ,  $q_0 = h\Delta\theta \cos\theta_B$ ,  $\alpha = 1$ ,  $\Delta\theta$  is the angular missetting from the Bragg angle  $\theta_B$ , and

$$2\pi = \frac{8\pi}{15} + \frac{\pi}{15} \frac{(3\nu^2 + 6\nu - 1)\cos\theta_B}{(1-\nu)^2} \quad (13)$$

The upper relation in Eq. (12) is for  $q_0 \leq \alpha/R_i$  and the lower for  $q_0 \geq \alpha/R_i$  where  $R_i$  is the radius of the  $i^{\text{th}}$  dislocation loop. Eq. (12) can be used to determine the loop size distribution through fitting the experimental measurements with  $C_i$  as parameters. Eq. (11) can be used with differential diffuse scattering measurements to determine the size and concentrations of defects in the same manner.

## Experimental Considerations

The study of defects ranging from single interstitial atoms to larger clusters and precipitates requires the use of a number of experimental configurations. One of the most useful and versatile configurations has been that of a focussed monochromating system using a curved monochromator crystal together with x-ray generators varying from 2 KW fixed anode systems to 15 KW rotating anode supplies. Several variations of the focussing geometry, such as shown in Fig. (2a), are used (4,7). The important aspect being the selection of only  $K\alpha_1$  radiation and the capability of varying the angular divergence of the incident beam (and hence the measurement resolution). This is done by limiting the width of the beam striking

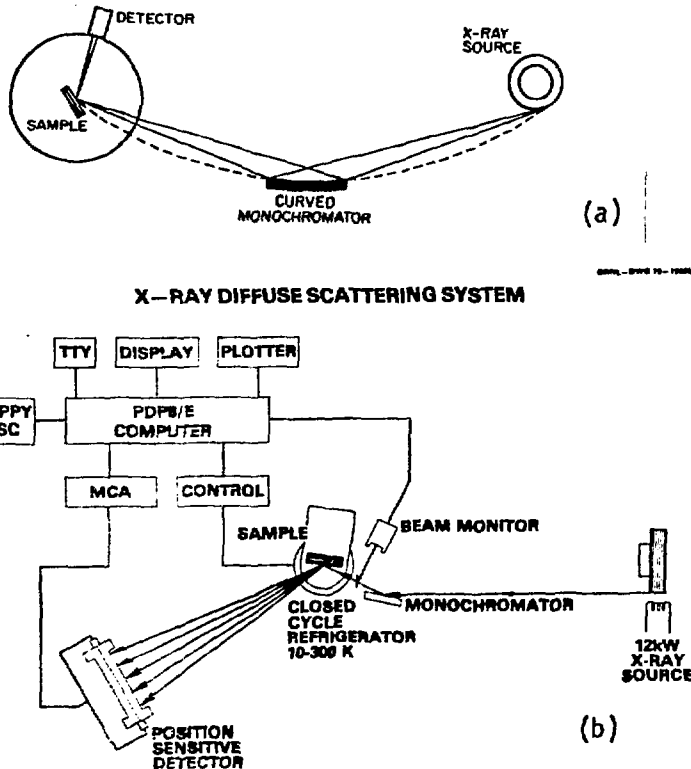


Fig. 2- a) Focused monochromator diffuse scattering geometry. b) Flat monochromator, diffuse scattering geometry with a position sensitive detector.

the curved monochromator crystal. For beam divergences  $0.1 - 1^\circ$ , incident beam powers of  $10^7 - 10^9$  photons/sec (depending on the vertical resolution) can be achieved and are adequate for Huang diffuse scattering from single  $10^3$  interstitials. In larger angle, point defect studies, beam powers  $> 5 \times 10^6$  photons/sec have been achieved using total reflecting mirrors in conjunction with an 100 KW x-ray source (5). Because of the low scattering rates between the Bragg reflections, a large multi-detector ( $\sim 100$ ) array was also necessary.

In the study of larger defect clusters, higher resolution is required and another technique employing a flat monochromator, 1 meter incident and diffracted beam distances and a position sensitive detector system has been used as shown in Fig. (2b). The relatively low beam power of  $\sim 10^6$  photons/sec realized in this scheme is offset by the position sensitive detector. Integral diffuse scattering measurements are considerably less demanding and

can be carried out with  $10^5 - 10^6$  photons/sec because of the large solid angle subtended by the detector. A 2 KW fixed anode generator and flat monochromators suffice for this geometry.

The sample requirements for diffuse scattering measurements discussed in this paper are first that they be single crystals. This can be a rather severe requirement for alloyed and compound materials, but has not proved to be too serious for pure materials. Sample sizes of  $0.5 \text{ cm}^2$  or greater are normally used, although smaller sizes are in principal possible in most cases. For detailed studies, the mosaic spread and subgrain misorientations must be  $<1/hR$  (where R is the defect radius) to ensure that q is well defined substantially into the Huang scattering region. For  $10 \text{ \AA}$  radius clusters, mosaic widths  $\sim 0.2^\circ$  would be possible, but for larger clusters, rather high quality crystals are required.

The subtraction of non-defect diffuse scattering must be carried out before analysis (4-7). This requires either identical crystals (one with and one without defects) or that measurements be made before and after the defects are introduced. Bragg reflections, Bragg tails, Compton scattering, and thermal diffuse scattering fall into this category. The thermal scattering can be minimized by measuring at temperatures  $\sim 10 \text{ K}$ .

### Measurement Results

#### Single Interstitials

Point defects can be characterized by x-ray diffuse scattering, through the symmetry of the distortion field surrounding the defect site and by the atomic configuration at the defect site. The symmetry of the distortion field is obtained from Huang diffuse scattering measurements close to reciprocal lattice points (small q), and the atomic configuration is determined from larger angle scattering between the Bragg reflections. As indicated in Eq. (7), Huang scattering measurements in appropriate directions lead to a determination (3) of the dipole-force tensor of interstitials and therefore differentiate between the several possible interstitial configurations. Without dealing in detail with the individual parameters in Eq. (7), measurements with  $\vec{q}$  parallel and perpendicular to  $\vec{h}$  at the (hoo), (hho) and (hhh) reflections provide all the obtainable information on the symmetry of the distortion field. As shown in Table I (4), cases of well defined symmetry can be determined by the identification of positions of zero Huang scattering.

Table I. Planes (P), Surfaces (S) or Lines (L) of Zero Huang Scattering for Characteristic Defect Symmetries.

Defect Symmetry	Reflection		
	(hoo)	(hho)	(hhh)
Cubic	P1 [100]	P1 [110]	S1 [111]
Tetragonal <100>	P1 [100]	L11 [011]	-
Trigonal <111>	-	L11 [110]	-
Orthorhombic <110>	-	-	-

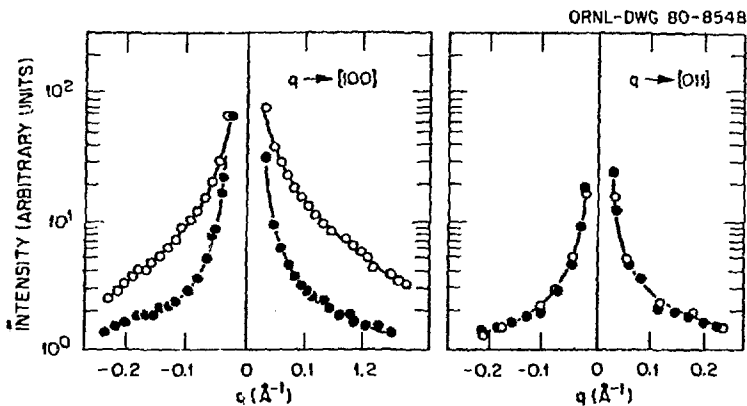
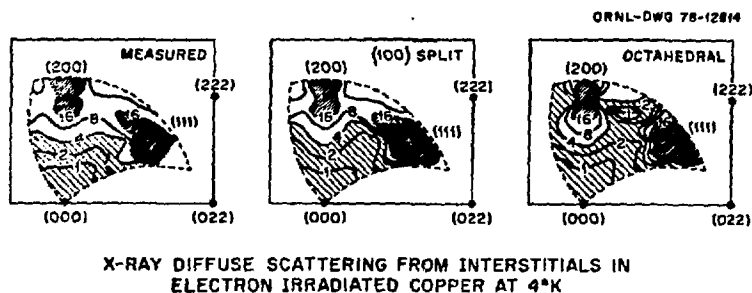


Fig. 3- Huang diffuse scattering at the 400 reflection from interstitials in electron irradiated (open circles) and unirradiated (filled circles) aluminum.

An application of the results of Table I is shown in Fig. (3). Interstitial scattering from low temperature electron irradiated aluminum was found (4) to be high along the  $[100]$  direction at the 400 reflection, but essentially zero along the  $[011]$  direction at this reflection. Of the cases listed in Table I, cubic and tetragonal symmetry would be allowed, and other measurements indicated that all configurations other than the  $\langle 100 \rangle$ -split interstitial, the octahedral, and the tetrahedral could be ruled out.

While lattice statics calculations have shown that each of these interstitial configurations have essentially cubic distortion fields (5), these configurations have significantly different atomic arrangements. Therefore the scattering at large angles between the Bragg reflections (which is quite sensitive to the Laue scattering) was able to show the  $\langle 100 \rangle$ -split interstitial to be the actual configuration. The same configuration was found for interstitials in copper (5) and Fig. (4) indicates the large angle scattering results (smoothed to emphasize the general features) supporting the  $\langle 100 \rangle$ -split interstitial in copper. The calculated intensity contours



X-RAY DIFFUSE SCATTERING FROM INTERSTITIALS IN ELECTRON IRRADIATED COPPER AT 4°K

Fig. 4- Large angle scattering from interstitials in electron irradiated copper, with calculated scattering for the  $\langle 100 \rangle$ -split and octahedral interstitial configurations.

were obtained using Eq. (3). The important result then, is that through scattering measurements both near-to and far-from Bragg reflections, single atom defects in the concentration range of  $10^{-4}$  -  $10^{-3}$  (atomic fraction) can be studied with diffuse scattering. These techniques apply to cases of gas atom interstitials and single sublattice interstitials as well as self interstitials, of course (7).

### Clustering of Point Defects

The clustering of point defects into 3-dimensional aggregates or dislocation loops can be observed in the symmetric averaged scattering  $[I(\vec{q})+I(-\vec{q})]/2$ , through the presence of a  $1/q^4$  falloff of the diffuse intensity at large  $q$  (as suggested by Eq. (10)) in addition to the  $1/q^2$  decrease of the intensity in the Huang region. This effect is shown clearly in Fig. (5) where 300 K thermal annealing of low temperature electron irradiated copper (14) is shown to result in increased intensity in the Huang region and a change to a  $1/q^4$  dependence for  $q/h > 0.005$ . The increased intensity results from the coherent scattering of point defects that have aggregated, compared to that for individual point defects scattering incoherently. According to the discussion of Eq. (10), the position ( $q_c$ ) of the transition to the  $1/q^4$  dependence provides an estimate of the cluster size (i.e.  $R_c \approx 1/q_c$ ); however, when distributions of sizes are present, this estimate can be rather misleading because of the weighting of the scattering by  $R^4$  and  $R^2$  in the Huang and asymptotic regions, respectively. As will be discussed below, direct fitting of detailed diffuse scattering calculations is necessary for accurate size determinations.

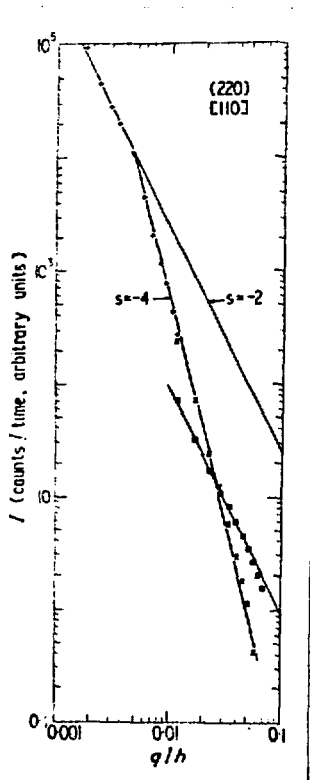


Fig. 5- Huang diffuse scattering from single interstitials (lower curve) and dislocation loops (upper curve) in electron irradiated copper at the 220 reflection with  $q$  along  $[110]$ .  $S$  denotes the slope of the lines.

## Diffuse Scattering Calculations for Dislocation Loops

Although the asymmetry in the Huang scattering intensity (Eq. (8)) can be used to differentiate between the presence of vacancy or interstitial loops, the  $R^4$  weighting of the intensities in the Huang region strongly biases the interpretation toward the larger loops. This makes it somewhat difficult to study small loops and clusters in the presence of large clusters. In the asymptotic region the weighting for loops is  $R^2$ , which gives equal scattering weight to loops with equal total areas. Therefore the intensity in this region is proportional to the number of point defects condensed into loops. This fact makes the asymptotic scattering more appealing for measurements, and detailed calculations for vacancy and interstitial loops on  $\{111\}$  planes in fcc materials have shown (12,15) the 222 reflection to be particularly favorable for distinguishing between vacancy and interstitial loops. This is indicated in Fig. (6) where contour plots of the scattering from 20 Å Frank loops of both vacancy and interstitial type are shown in a form multiplied by  $q^4$  to remove the average  $1/q^4$  falloff. The important result is the peak in the scattering at  $q > 0$  for interstitial loops and at  $q < 0$  for the vacancy case. This peaked intensity has been identified as Bragg-like scattering from the strained region near the loops, and because the magnitude of the strain in this region is  $\epsilon \approx -b/4R$ , this peak can be expected at (12)

$$q = -\epsilon h \approx \frac{bh}{4R} \quad (14)$$

Not only is the vacancy-interstitial nature of the loop specified, but also the size can be determined through comparisons with numerical scattering calculations, since  $\epsilon$  is a function of  $R$ .

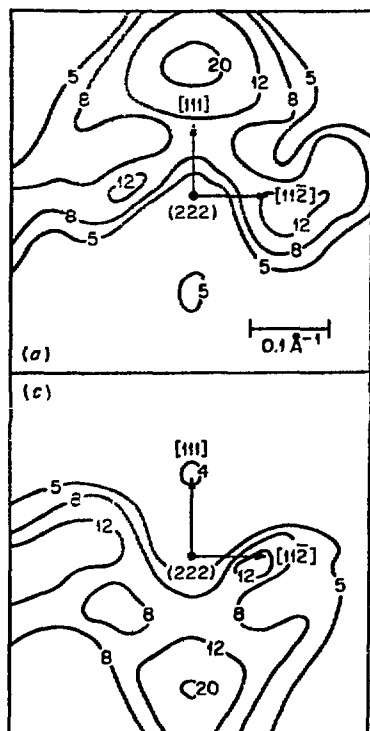


Fig. 6- Calculated diffuse scattering intensity (multiplied by  $q^4$ ) for Frank loops of interstitial (upper) and vacancy (lower) loops at the 222 reflection in an isotropic material.

## Vacancy and Interstitial Loop Size Distributions

The above characteristics were observed in earlier calculations (12) and were seen experimentally (16) on 4 K electron irradiated copper that had been annealed to 200 K. The presence of interstitial type loops in copper (at 200 K) resulted in a highly asymmetric scattering similar to that indicated in Fig. (6a). Calculations for anisotropic crystals have been carried out using anisotropic displacement field data as generated by Ohr (17). Similar results were obtained. These anisotropic calculations have been applied to the analysis of diffuse scattering measurements from copper irradiated with 60-MeV Ni ions at 300 K. Scattering measurements for  $\vec{q}$  along [111] near the 222 reflection are shown in Fig. (7) and the analysis of this scattering is shown in Fig. (8). These results, shown here for the first time, demonstrate the size distribution and concentration determination possibilities using this technique. The details of the measurement and analysis will be published elsewhere. The observation of nearly equal intensities for  $q > 0$  and  $q < 0$  in Fig. (7) indicates, qualitatively, the presence of both types of loops in the sample, while the differences in the shapes and positions of the maxima imply the vacancy loops are smaller than the interstitials (recall that the vacancy loop scattering is predominantly at  $q < 0$ ). Fitting of these data with numerical calculations for vacancy and interstitial loops of 10, 20, 30, 40 and 60 Å sizes and treating the concentration of each loop size and type as parameters, lead to the size distributions in Fig. (8). Although the fitting was done with five specific sizes, the results have been (artificially) spread over 10 Å ranges and reduced to units of loops/cm<sup>3</sup>/Å (the 60 Å result is spread over 30 Å) so that the area under Fig. (8) yields the total loop concentrations.

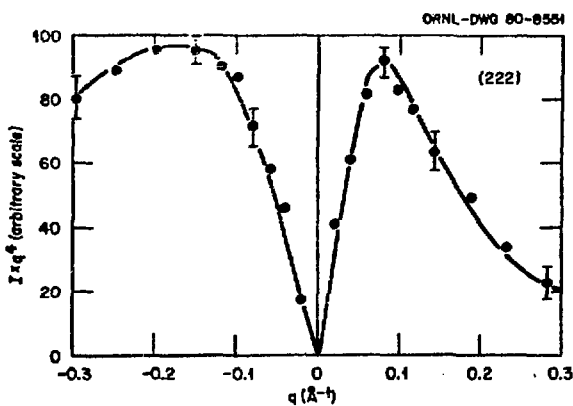


Fig. 7- Measured diffuse scattering from ion irradiated copper at the 222 reflection.

The vacancy loops can be seen to have smaller sizes than the interstitial loops, but the significantly larger numbers of vacancy loops offset the size difference such that the number balance of point defects in the combined distribution turns out to be 53.5% vacancies and 46.5% interstitials. These values may be considered equal within the estimated uncertainties ( $\pm 7\%$ ) of the analysis and therefore suggest that all the vacancies are condensed into dislocation loops. Existing electron microscopy results on copper, irradiated under various conditions have been inconclusive on this point, reporting values ranging from a factor of two to less than half as many vacancies in loops as interstitials in loops (18,19). Fig. (9) is a semi-log plot of the combined size distribution together with published (20) TEM results superposed for comparison. Both results refer to the damage peak region near the end of range of the ions (20). The agreement in the larger sizes is quite

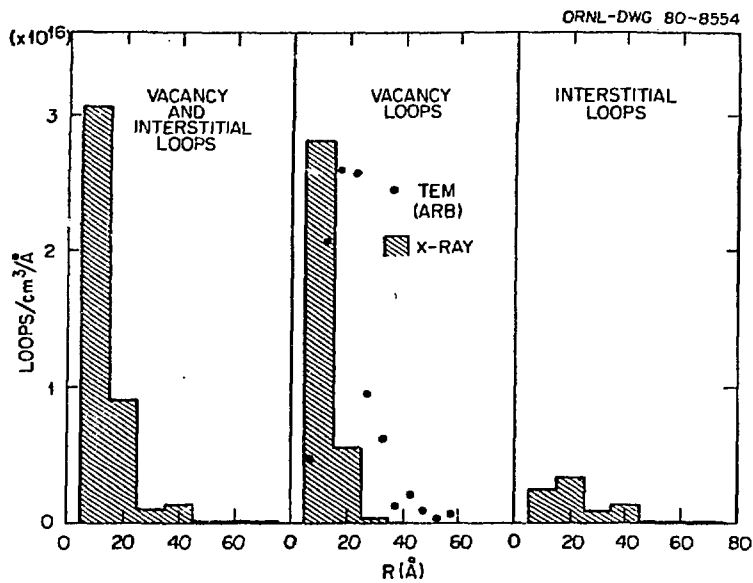


Fig. 8- Size distribution for loops in ion irradiated copper obtained from the x-ray diffuse scattering in Fig. (7). The TEM results are for vacancy loops in 30 KeV Cu irradiated copper (21). The TEM vertical scale is arbitrary.

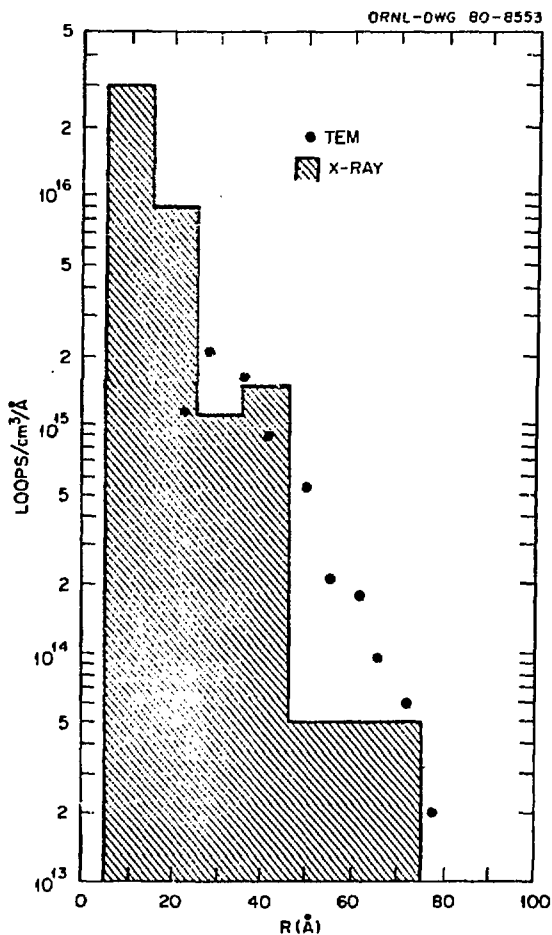


Fig. 9- Combined size distribution of vacancy and interstitial loops from Fig. 8, with TEM results on a similarly irradiated crystal (20).

reasonable, but the correspondence is not very good for small sizes, which are predominantly composed of vacancy loops in the x-ray results. A direct comparison of the vacancy loop distribution determined by x-rays with vacancy loops imaged by TEM in low energy (30 KeV) copper ion irradiated copper (21) at 293 K, is made in Fig. (8). These microscope results are scaled arbitrarily, so only the size of the loops and the shape of the distribution are of significance. Although the microscope result indicates slightly larger sizes than does the diffuse scattering, both methods show rather narrow distributions. Considering the differences in irradiation conditions, the close similarity in the results seems encouraging. However, this is the first direct comparison of the size distributions of the individual dislocation loop types determined by x-rays with those from TEM, so firm conclusions about the above results may be somewhat premature.

### Loops and Precipitates

Huang diffuse scattering can be used to differentiate between planar loops and three dimensional precipitate clusters in a manner similar to that applied in point defect symmetry determinations (see Table I). An example of this is shown in Fig. (10) where the Huang diffuse scattering from dislocation loops in neutron irradiated copper and cobalt precipitates in Cu(1%)Co are shown (22). Characteristic differences can be seen between the scattering in the two cases. The scattering is rather isotropic from the dislocation loops while the precipitate scattering perpendicular to the [100] direction tends to vanish. In addition, the asymmetry in the scattering, along the [100] direction, has the opposite sense for the cobalt precipitates, compared to that for the loops. From Table I, it can be seen that these measurements would rule out cubic or tetragonal defects in the neutron irradiation case and rule out trigonal or orthorhombic defect symmetry in the precipitate case. Measurements at the 111 reflection completed the characterization as cubic or spherical symmetry for the precipitates and {111} loops in the case of the neutron irradiated copper. Both of these results---

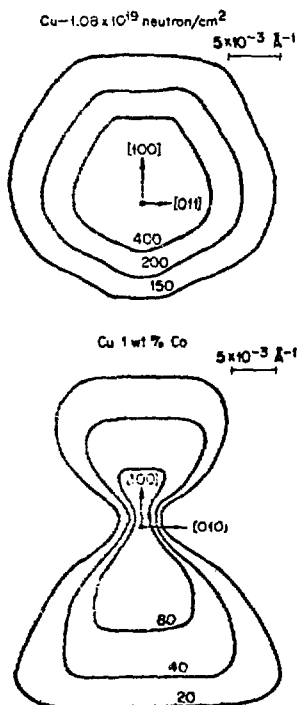


Fig. 10- Huang scattering from dislocation loops (upper) in neutron irradiated copper and precipitates (lower) in 570°C aged Cu(1%)Co.

are in agreement with known electron microscopy results (22,23) for these systems. The higher intensity for  $q>0$  in the loop case and higher intensity for  $q<0$  in the cobalt scattering can be related to the second term in Eq. (8) and indicates the cobalt precipitates cause an inward displacement of the lattice surrounding them, while the asymmetry in the loop scattering indicates an outward displacement. An outward displacement implies interstitial loops; however, since vacancy loops are known to be present as well, the larger sizes of the interstitial loops in connection with the  $R^4$  scaling can be assumed to cause them to dominate the scattering. This possibility was discussed in the calculational paragraph above.

### Diffuse Scattering from Coherent Precipitates

Although a considerable amount of small angle scattering (forward direction) has been directed toward the study of precipitates, x-ray scattering near Bragg reflections has received relatively little attention in this regard. The characteristic features associated with scattering from precipitates can be seen in the calculations shown in Fig. (11). These calculations were based on Eq. (5), using  $f_h = f_D$  for simplicity, and choosing the strain inside the precipitate to be  $-0.014$ , the radius to be  $70 \text{ \AA}$  and assuming an isotropic crystal with the lattice parameter of copper.  $\vec{q}$  is along the (400) reciprocal lattice vector. The important features in the scattering are the  $1/q^2$  Huang scattering region, the asymmetry (corresponding to inward displacements) caused by the strain  $\epsilon = -0.014$ , the oscillating intensity for  $q<0$  with a  $1/q^4$  falloff of the envelope, and the smoothly varying intensity for  $q>0$  with a shoulder at  $q \sim 0.1 \text{ \AA}^{-1}$ . The oscillations

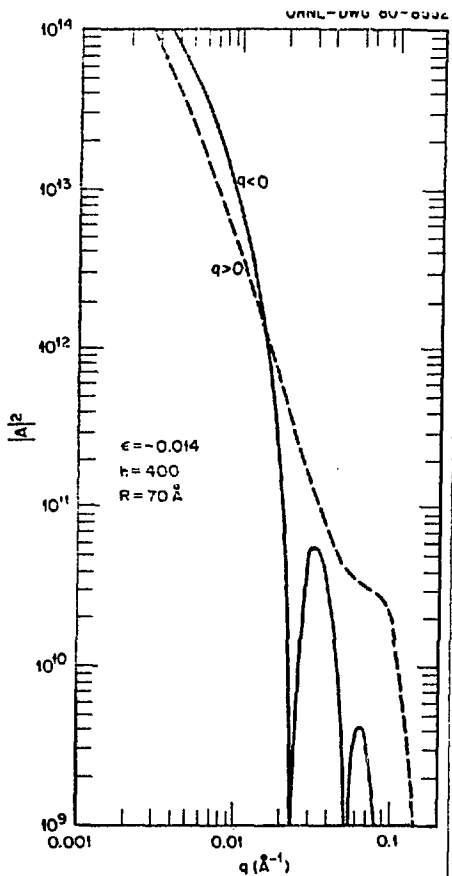


Fig. 11- Calculated diffuse scattering from spherical precipitates in an isotropic crystal.

are a result of interferences (10) in the scattering from the highly strained region outside the precipitate, and the shoulder at  $q \sim 0.1 \text{ \AA}^{-1}$  can be shown to result from the Laue scattering from the precipitate particle. Experimental identification of this shoulder position can then be used to measure the strain inside the particle as

$$\epsilon = -q/h \tag{14}$$

Measurements on Cu(1%)Co have shown (24) the existence of a shoulder at  $q \sim 0.1 \text{ \AA}^{-1}$  which would appear to be consistent with a TEM measurement of  $\epsilon = -0.014$  using Moire fringe measurements (25). However, Fig. 11 does not consider the anisotropy of the copper lattice so this comparison cannot be regarded as complete. The possibility of measuring the misfit strain inside the particle is demonstrated, though, and further work should allow size and concentration determinations using anisotropic calculations.

### Integral Diffuse Scattering

Although differential diffuse scattering measurements (which are characterized by a single scattering vector,  $\vec{K}$ ) provide the most detailed information about defect structures and are the most amenable to numerical calculations for analyses, integral diffuse scattering (6,13,26,27) as illustrated in Fig. 1b) can be useful also. Because of the integration of the intensity over a large solid angle (limited in effect by the range of the scattering for clustered defects) accurate measurements can be made with modest equipment. However, the approximations associated with Eq. (12) and the symmetric averaging  $(I(\Delta\theta)+I(-\Delta\theta))/2$  result in the loss of vacancy-interstitial type determinations, and the detailed calculations using Eq. (2) enter only indirectly through integration. Nevertheless, as shown in Fig. (12a, b) for neutron irradiated copper (6), results can be obtained that yield

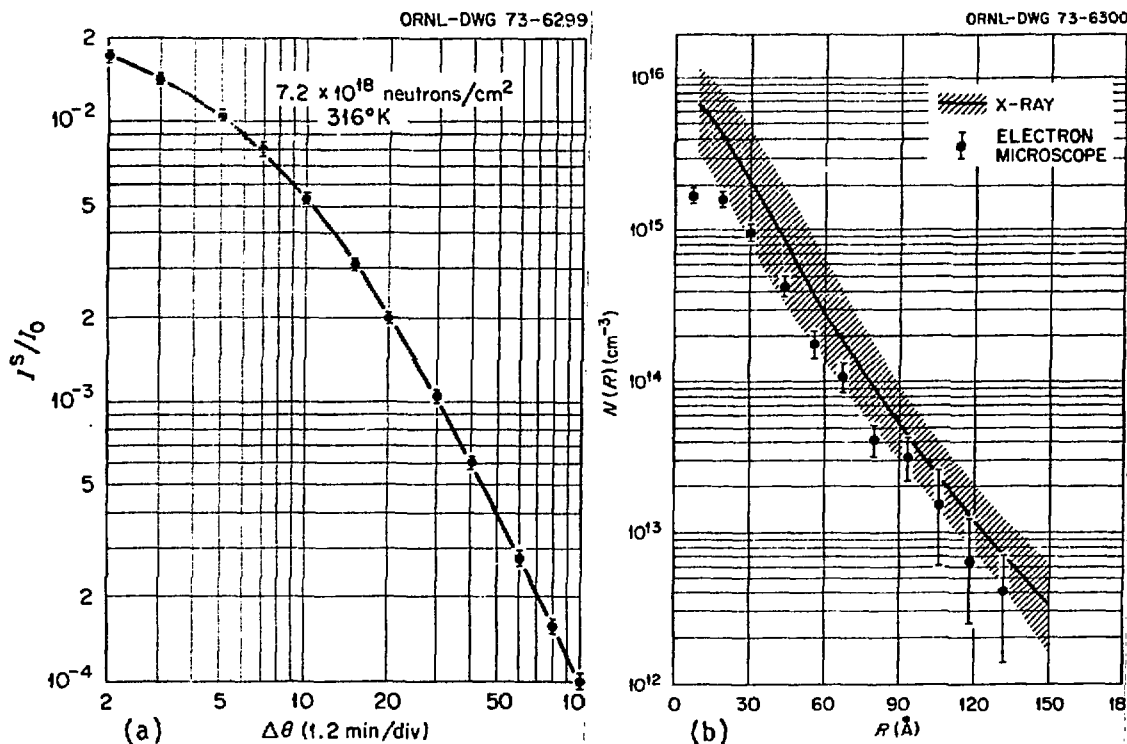


Fig. 12- a) Integral diffuse scattering at the 111 reflection from neutron irradiated copper b) Size distribution of dislocation loops obtained from (a) with TEM results on a similarly irradiated sample.

dislocation loop concentrations and size distributions. Fig. (12a) contains integral diffuse measurements on copper irradiated with  $7.2 \times 10^{18}$  n/cm<sup>2</sup> at 316 K. The logarithmic  $q_0$  dependence at small  $q_0$  can be seen, as can the  $1/q_0^2$  dependence for larger  $q_0$ . The results of fitting the data in Fig. (12a) yielded the size distribution in Fig. (12b) (solid line). These results compare favorably with the electron microscopy results on a similarly irradiated sample shown as the solid circles. It is interesting to notice that in this case, as well as in Fig. (9), the largest discrepancy occurs at the small sizes. This method has been employed in studies of dislocation loops in electron, neutron, and ion irradiated metals, and in cases where comparisons with electron microscopy could be carried out (12), similar results to those in Fig. (12b) were obtained. Direct comparisons of integral diffuse scattering and differential diffuse scattering results are in progress. As suggested by Fig. (9); however, the high concentrations of small loops seem to be present in both the integral and differential methods of investigations.

### Conclusion

We have seen that diffuse scattering can be used effectively in investigations of defects as small as single interstitials up to defect clusters that could, in principle, range to several hundred Angstroms. Larger clusters are not precluded (27), but will in general require special considerations on measuring resolution and crystal perfection. In order to make a rough overall evaluation of the diffuse scattering technique compared to the electron microscope technique for studying these defects, positive (+) and negative (-) aspects of both techniques are listed in Table II.

Table II. Positive (+) and Negative (-) Aspects of Diffuse Scattering and Electron Microscopy techniques.

X-Ray Diffuse Scattering		Electron Microscopy	
+	-	+	-
Non-destructive technique	Single crystals required	Polycrystalline or single crystal	Destructive technique
Good statistics inherent	higher concentrations required	Lower concentrations possible	Good statistics tedious
Sensitive to point defects	>500 A sizes difficult	Larger sizes possible (sample limited)	>10 A sizes required
Bulk property measurement	Results require analysis	Direct observation (usually)	Thin samples (non-bulk)

From this table it would appear that initial survey work, investigations of larger defects, and studies where concentration levels are likely to be low, would clearly favor the use of electron microscopy. For studies of small defects, investigations where subtle changes in defect sizes or concentrations are of interest, and when measurements are required after sequential sample treatments, such as isochronal annealing or ageing, the diffuse scattering technique offers significant advantages. An overall examination of Table II indicates that in many ways, diffuse scattering and electron microscopy are complementary tools. Although the study of point defects and very small clusters by diffuse scattering requires a significant

experimental effort, this size region is inaccessible by electron microscopy so that such an effort is justified. The availability of synchrotron radiation sources and the construction of sophisticated scattering equipment at synchrotron sites will, however, significantly reduce the barriers for presently, difficult diffuse scattering measurements and make these experiments within the capabilities of a much larger community.

Because of the requirement of single crystal samples with little or no deformation tolerable, diffuse scattering measurements are not well suited for studying uncharacterized samples such as obtained from structural components. Rather, the power of diffuse scattering is realized by devising experiments, (on controlled and well characterized samples) that will provide information of general application. This is, of course, the philosophy of fundamental defect studies in any case.

The technique of obtaining the size distribution of vacancy loops separate from interstitial loops by diffuse scattering would appear to be a particularly useful contribution. Although electron microscopy has this capability, it is a very tedious process that tends to inhibit its routine use for small loops. The development of theoretical diffuse scattering calculations, for analysis of scattering measurements, has played an important role in the loop studies, and will continue to play a critical role in the further development of defect studies by diffuse scattering. As the capabilities of the diffuse scattering technique improve, it will be increasingly important to make use of coordinated investigations of defects and defect structures, by both diffuse scattering and TEM, in order that the most desirable attributes of both techniques may be exploited.

#### Acknowledgement

The author would like to thank J. F. Barhorst for help in collecting and analyzing some of the data presented in this paper.

#### References

1. M. A. Krivoglaз, Theory of X-Ray and Thermal Neutron Scattering by Real Crystals, Plenum Press, New York, 1969.
2. P. H. Dederichs, "The Theory of Diffuse X-ray Scattering and its Application to the Study of Point Defects and their Clusters," J. Phys. F: Metal Phys. 3, (1973) pp. 471-496.
3. H. Trinkaus, "On the Determination of the Double-Force Tensor of Point Defects in Cubic Crystals by Diffuse X-ray Scattering," Phys. Stat. Sol. (b), 51, (1972) pp. 307-319.
4. P. Ehrhart and W. Schilling, "Investigation of Interstitials in Electron Irradiated Aluminum by Diffuse X-ray Scattering Experiments," Phys. Rev. B8, (1974) pp. 2604-2621.
5. H. -G. Haubold, "Study of Irradiation Induced Point Defects by Diffuse Scattering," pp. 268-283 in Fundamental Aspects of Radiation Damage, M. T. Robinson and F. W. Young, Jr., ed.; ERDA CONF-75 1006 - P1, Oak Ridge, TN, 1976.
6. B. C. Larson, "X-ray Studies of Defect Clusters in Copper," J. Appl. Cryst. 8, (1975) pp. 150-160.

7. H. Peisl, "X-ray Scattering from the Displacement Field of Point Defects and Defect Clusters," *J. Appl. Cryst.* 8, (1975) pp. 143-149.
8. B. von Guerard and J. Peisl, "Diffuse X-ray Study from Copper after Neutron Irradiation at 4.6 K," pp. 287-294 in (same as Ref. 5).
9. M. Moringa and J. B. Cohen, "The Defect Structure of VO<sub>2</sub>. II. Local Ionic Arrangements in the Disordered Phase," *Acta. Cryst.* A35, (1979) pp. 975-989.
10. H. Trinkaus, "Der Reflexferne Teil der Diffusen Streuung von Roentgenstrahlen," *Z. Angew. Phys.* 31, (1971) pp. 229-235.
11. H. -G. Haubold and D. Martinsen, "Structure Determination of Self-Interstitials and Investigation of Vacancy Clustering in Copper by Diffuse X-ray Scattering," *J. Nucl. Mat.* 69,70 (1978) pp. 644-649.
12. B. C. Larson, "X-ray Studies of Irradiation Induced Dislocations in Metals," pp. 820-238, in (same as Ref. 5).
13. B. C. Larson and F. W. Young, Jr., "A Comparison of Diffuse Scattering by Defects Measured in Anomalous Transmission and Near Bragg Reflections," *Zeit. Naturforsch.* 28a (1973) pp. 626-632.
14. P. Ehrhart, H. -G. Haubold, and W. Schilling, "Investigation of Point Defects and their Agglomerates in Irradiated Metals by Diffuse X-ray Scattering," *Advances in solid State Physics*, 14 (1974) pp. 87-110.
15. P. Ehrhart and B. C. Larson, "Calculation of Diffuse Scattering from Dislocation Loops," Annual Progress Report, Solid State Division, Oak Ridge National Lab., Oak Ridge, TN, (1977) pp. 84-85.
16. P. Ehrhart and V. Schlagheck, "Investigation of Interstitial Clusters in Copper by Measurement of the Huang Diffuse Scattering," pp. 839-845 in (same as Ref. 5).
17. S. M. Ohr, "Displacement Field of a Dislocation Loop in Anisotropic Cubic Crystals," *Phys. Stat Sol. (b)* 64, (1974) pp. 317-323.
18. M. Rühle, F. Häusermann, and M. Rapp, "Transmission Electron Microscopy of Point Defect Clusters in Neutron Irradiated Metals," *Phys. Stat. Sol.* 39 (1970) pp. 609-620.
19. J. Narayan and S. M. Ohr, "The Nature of High Energy Neutron Damage in Copper and Gold," *J. Nucl. Mat.* 85,86 (1979) 515-519.
20. J. B. Roberto and J. Narayan, "Ni Ion Damage in Cu and Nb," pp. 120-126 in (same as Ref. 5).
21. C. A. English, B. L. Eyre, J. Summers, and H. Wadley, "The Behavior of Collision Cascades at Elevated Temperatures in Copper and Molybdenum Crystals," pp. 910-917 in (same as Ref. 5).
22. B. C. Larson and W. Schmatz, "Huang Diffuse Scattering from Dislocation Loops and Cobalt Precipitates in Copper," *Phys. Rev.* B10 (1974) pp. 2307-2314.

23. H. P. Degischer, "Diffraction Contrast from Coherent Precipitates in Elastically Anisotropic Materials," *Philos. Mag.*, 26 (1972) pp. 1137-1152.
24. W. Schmatz and B. C. Larson, unpublished.
25. C. G. Richards and W. M. Stobbs, "Determination of *in situ* Misfits of Coherent Particles," *J. Appl. Cryst.* 8 (1975) pp. 226-228.
26. B. C. Larson and F. W. Young, Jr., "Effect of Temperature of Irradiation Induced Dislocations in Copper," *J. Appl. Phys.* 48 (1977) pp. 880-886.
27. J. R. Patel, "X-ray Diffuse Scattering from Silicon Containing Oxygen Clusters," *J. Appl. Cryst.* 8 (1975) pp. 186-190.